Supplementary Information (SI) for Materials Horizons.
This journal is © The Royal Society of Chemistry 2026

Supporting Information

Unlocking the Role of Indium Ions to Stabilize Zinc Negative Electrodes in Highly Acidic Electrolytes for High-Voltage Aqueous Zn Batteries

Ting-Yu Wang[a], Hung-Yi Huang[a], Yi-Heng Tu[a], Yi-Cheng Liao[a], Chi-Yu Lai[a], Timo Jacob[b, c, d], Mohamed M. Elnagar[b, c, d], Mohammad Al-Shakran[b], Chi-Chang Hu[a, e, f, *]

Submitted to
Materials Horizons

*Corresponding Author: Chi-Chang Hu, Email: cchu@che.nthu.edu.tw, NTHU Chair Professor

[a]Department of Chemical Engineering, National Tsing Hua University, Hsinchu 300044, Taiwan

[b]Institute of Electrochemistry, Ulm University, 89081 Ulm, Germany

[c]Helmholtz-Institute-Ulm (HIU) Electrochemical Energy Storage, 89081 Ulm, Germany

[d]Karlsruhe Institute of Technology (KIT), P.O. Box 3640, 76021 Karlsruhe, Germany

[e]College of Semiconductor Research, National Tsing Hua University, Hsinchu 300044, Taiwan

[f]College of Sustainability, National Tsing Hua University, Hsinchu 300044, Taiwan

Keywords: high voltage batteries, highly acidic, additives, In-Zn binary alloy, indium ions

This supporting information consists of 17 pages, including 15 figures and 5 tables.

Methods:

1. Materials:

All reagents and materials in this work are commercially available and were used without further purification. Zinc sulfate heptahydrate ($ZnSO_4 \cdot 7H_2O$, ≥99%), manganese sulfate monohydrate ($MnSO_4 \cdot H2O$, ≥99%), indium sulfate ($In_2(SO_4)_3$), Zn foil (≥99%), graphite (Cetech, 25 um thickness), sulfuric acid (H_2SO_4).

2. Cell assembly and electrochemical measurements

Zn||Zn symmetric coin cells were assembled using Zn foils (thickness ≈ 100 μm) as electrodes, with a glass fiber separator (Whatman, 0.26 mm thick) and 60 μL of electrolyte (1 M $ZnSO_4$ + 0.1 M H_2SO_4 with or without indium sulfate) per cell. Cuvette and beaker cells were prepared using the same Zn foils as electrodes, containing 2 mL and 10 mL of the same electrolyte, respectively, depending on the experimental requirements. Zn||graphite coin cells were assembled similarly, with one Zn electrode replaced with a graphite paper.

Acidic Zn||MnO_2 coin cells were assembled using a Zn negative electrode (1.539 cm^2) and an acid-washed carbon felt positive electrode (1.13 cm^2, 2 mm thickness, CeTech Ltd.) with an electrolyte of 1 M $ZnSO_4$ + 1 M $MnSO_4$ + 0.3 M H_2SO_4, with or without 5 mM indium sulfate. The cells were charged at 30 mA cm^{-2} to 0.2 mAh cm^{-2} and discharged at 5 mA cm^{-2} to a cutoff voltage of 1.0 V. The acidic Zn||MnO_2 pouch cell was constructed using the same Zn negative electrode (1.539 cm^2) and a positive electrode composed of activated carbon with graphene additive (ACUG; Ultra-Graphene, Nanotech Energy Inc.), with the same electrolyte composition, with or without 5 mM indium sulfate. These cells were charged at 30 mA cm^{-2} to 0.325 mAh cm^{-2} and discharged at 5 mA cm^{-2} to 0.3 V. Zn||PbO_2 batteries was constructed using the commercial PbO_2 electrodes (1 cm^2, Coommee Industrial Co., LTD.) as the positive electrode and Zn (2 cm^2) as the negative electrode, with 1 M $ZnSO_4$ + 2 M H_2SO_4 electrolyte, with or without 5 mM indium sulfate. All Zn||PbO_2 batteries were assembled in 4 mL commercial cell containers (Coommee Industrial Co., LTD.) and tested by charging at 4 mA cm^{-2} to 0.5 mAh cm^{-2}, followed by discharge at 10 mA cm^{-2} to 2.2 V.

All coin cells were tested in CR2032 coin-type configurations, sealed under a pressure of 50 kg cm^{-2}.

The symmetric cell, coulombic efficiency, and full-cell tests were carried out on a LAND CT2001A battery testing system, all at 25 °C. Additional electrochemical analyses, including cyclic voltammetry (CV), linear sweep voltammetry (LSV), and the three-

electrode configuration were performed using a Bio-Logic workstation.

3. Characterizations

Morphological characteristics were examined using the field-emission scanning electron microscopy (FESEM, Hitachi SU8010), and crystallographic information of Zn electrodes was obtained via the X-ray diffraction (XRD, D8 Advance A25, Bruker, Germany). The surface composition were examined through high-resolution X-ray photoelectron spectroscopy (HRXPS, ULVAC-PHI, PHI Quantera II). A focused ion beam-scanning electron microscopy (FIB-SEM, ThermoFisher, USA) coupled with energy-dispersive X-ray spectroscopy (EDX, Ametek, USA) was carried out. A gallium (Ga) ion beam source with a beam current of 1.5 nA (at 20 keV) was used for cross-sectional analysis via surface milling. The Time-of-Flight Secondary Ion Mass Spectrometer (TOF-SIMS, ION-TOF, Germany) was employed to provide a detailed assessment of the depth-dependent distribution of indium.

4. Computational methods

All theoretical calculations were conducted using the density functional theory (DFT) via the Materials Studio software. The electron-ion interactions were interpreted by the projected augmented wave (PAW) method, while the exchange-correlation energy was described by the scheme of Perdew-Burke-Ernzerhof (PBE) in the generalized gradient approximation. The cutoff energy was set to 500 eV and the k-points setting is 15 × 8 × 1. The crystal surfaces were constructed by the usage of the slab model with a symmetric slab containing a vacuum layer (>15 Å), which can avoid interactions between adjacent slabs. The atomic relaxation wave was stopped when the total energy tolerance was converged to 2×10^{-5} eV and the changes of the force on atoms were less than 0.05 eV $Å^{-1}$.

Binding energies (E_b) were calculated as

$$E_b = E_{\text{total}} - E_{\text{surface}} - E_{\text{adsorbate}}$$

where E_{total}, E_{surface} and $E_{\text{adsorbate}}$ are the energies of the full system, clean surface, and isolated adsorbate, respectively. The more negative E_b value indicates the stronger adsorption.

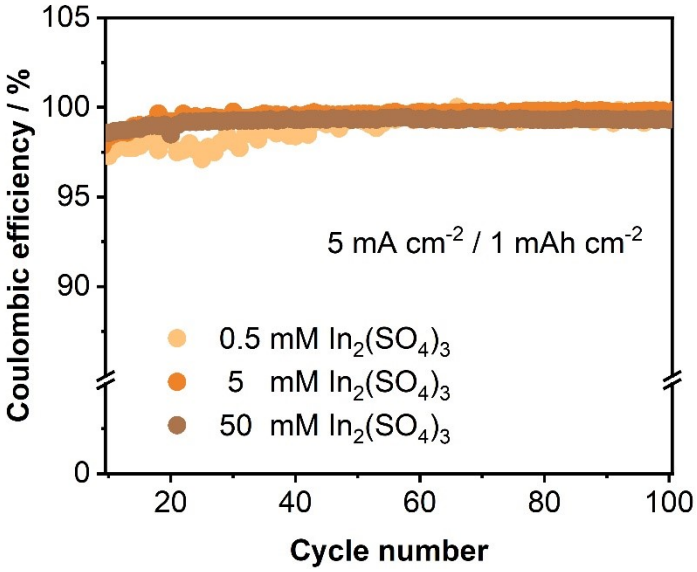

Figure S1. The coulombic efficiency-cycle profiles of Zn plating/stripping at 5 mA cm^{-2} and 1 mAh cm^{-2} with three indium sulfate concentrations.

To optimize the concentration of indium sulfate, the Zn plating/stripping CE measurement was first conducted on graphite paper at a current density of 5 mA cm^{-2} with an areal capacity of 1 mAh cm^{-2} using electrolytes containing various indium sulfate concentrations. As shown in Figure S1, the electrolyte with 5 mM indium sulfate exhibits significantly more stable CE values than that with 0.5 mM indium sulfate, while delivering a performance comparable to that obtained in the electrolyte with 50 mM indium sulfate. Considering that electrolyte additives are generally preferred to be effective at the lowest possible concentration in order to minimize cost and potential side effects, 5 mM was therefore selected as the optimal and practical In^{3+} concentration for the subsequent studies.

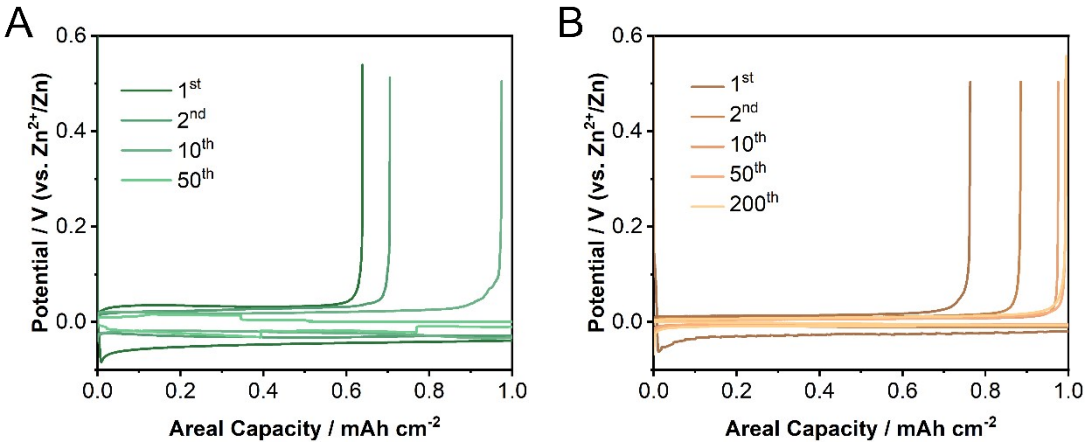

Figure S2. The galvanostatic charge-discharge voltage profiles of Zn plating/stripping at 1 mA cm^{-2} and 1 mAh cm^{-2} over various cycles in (A) ZSO and (B) ZSO/In^{3+} electrolytes.

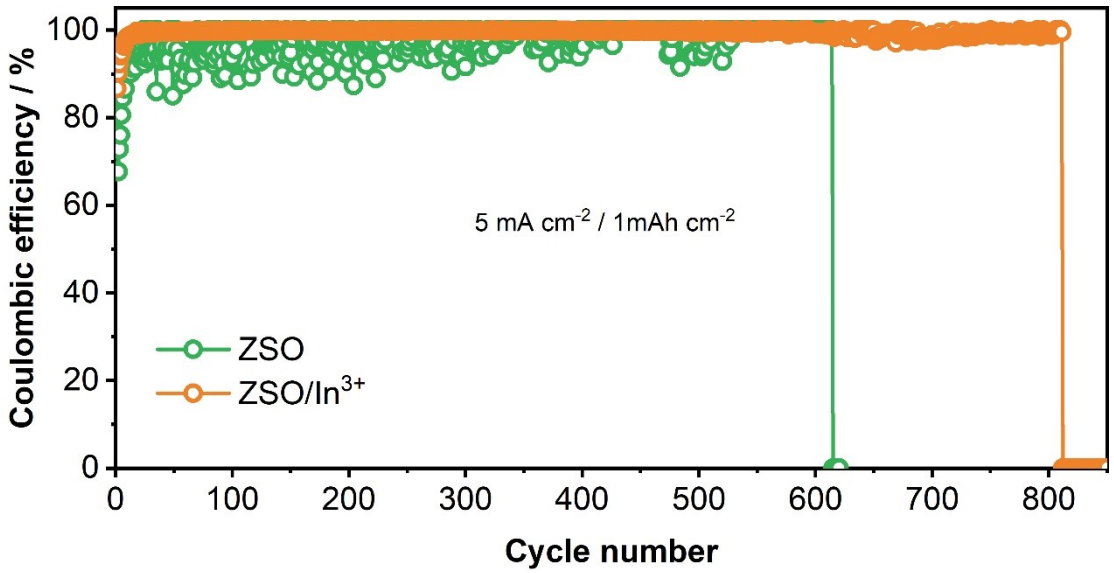

Figure S3. The coulombic efficiency-cycle profiles of Zn plating/stripping at 5 mA cm^{-2} and 1 mAh cm^{-2} in ZSO and ZSO/In^{3+} electrolytes.

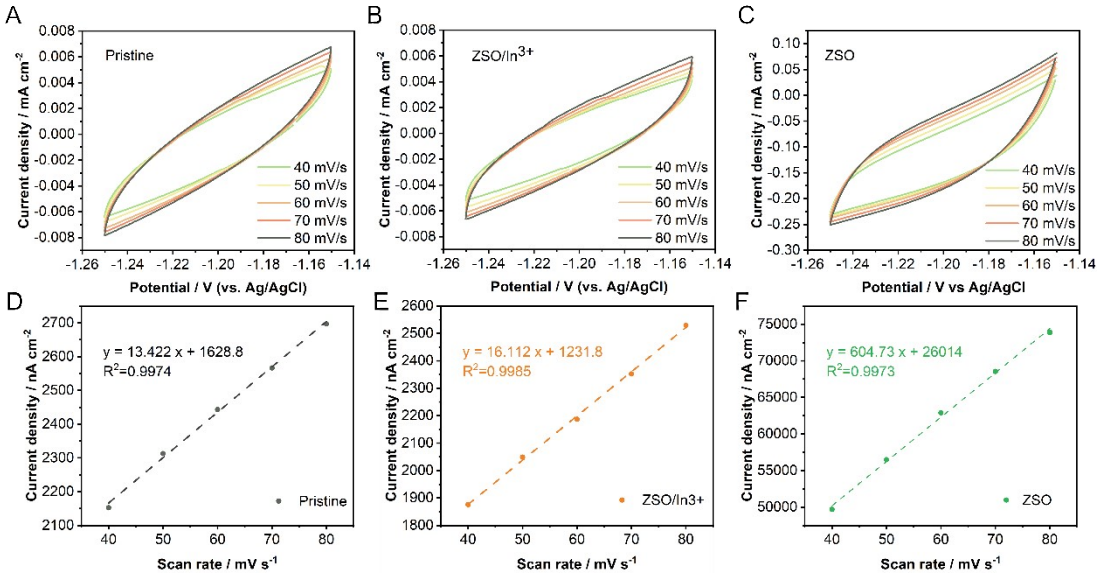

Figure S4. Cyclic voltammograms recorded at various scan rates (40–80 mV s^{-1}) in 1 M Na_2SO_4 using (A) pristine Zn and Zn in (B) ZSO/In^{3+}, and (C) ZSO. Panels (D–F) show the corresponding linear fittings of the double-layer current versus scan rate.

Areal capacitance calculation detail:

Areal capacitance measurements were performed using pristine Zn and Zn electrodes cycled in ZSO and ZSO/In^{3+} electrolytes at a current density of 1 mA cm^{-2} with an areal capacity of 1 mAh cm^{-2} for 10 cycles as the working electrodes. A Pt wire and an Ag/AgCl electrode were used as the counter and reference electrodes, respectively. All measurements were conducted in 1 M Na_2SO_4 to exclude Zn^{2+} participation and suppress the interference from the hydrogen evolution reaction (HER). Cyclic voltammetry (CV) was performed within the non-Faradaic potential window at scan rates from 40 to 80 mV s^{-1} to ensure no redox reactions for evaluating the double-layer capacitance. At a fixed potential of 1.2 V versus Ag/AgCl, the double layer current was estimated as the cathodic current minus the anodic current divided by two, which helps minimize the interference from any unknown background currents. The resulting currents were then plotted as a function of the scan rate, and the slope of the linear fit corresponds to the double-layer capacitance.[1, 2]

$$i_{dl} = \frac{i_{cathodic} - i_{anodic}}{2}$$

$$C_{dl} = \frac{di}{dv}$$

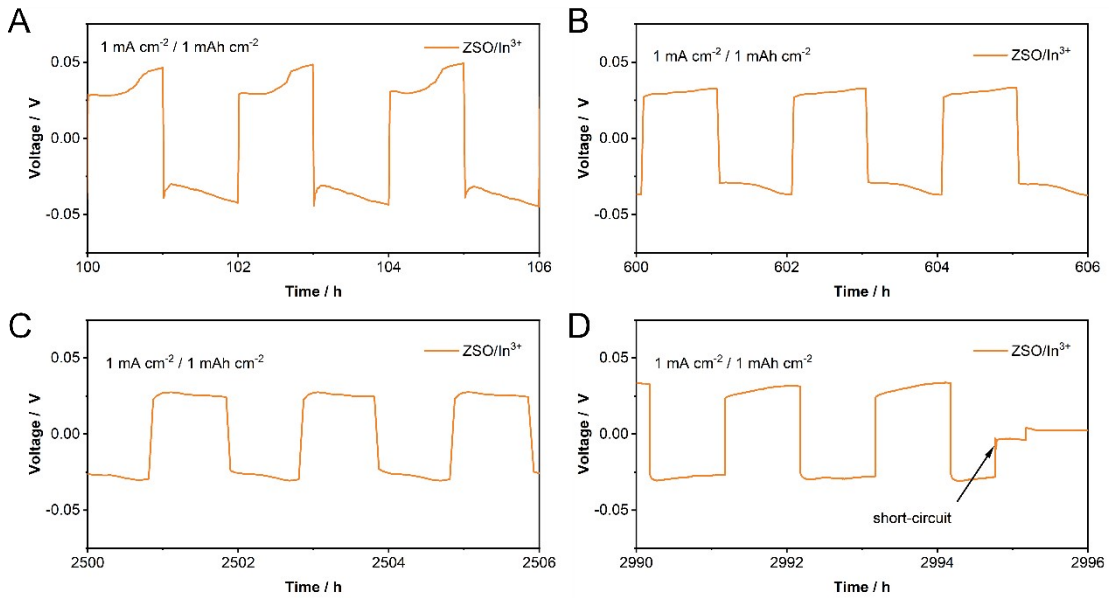

Figure S5. Enlarged voltage profiles of the Zn||Zn symmetric cells in the ZSO/In^{3+} electrolyte at selected cycling intervals: (A) 100–106 h, (B) 600–606 h, (C) 2500–2506 h, and (D) 2990–2996 h.

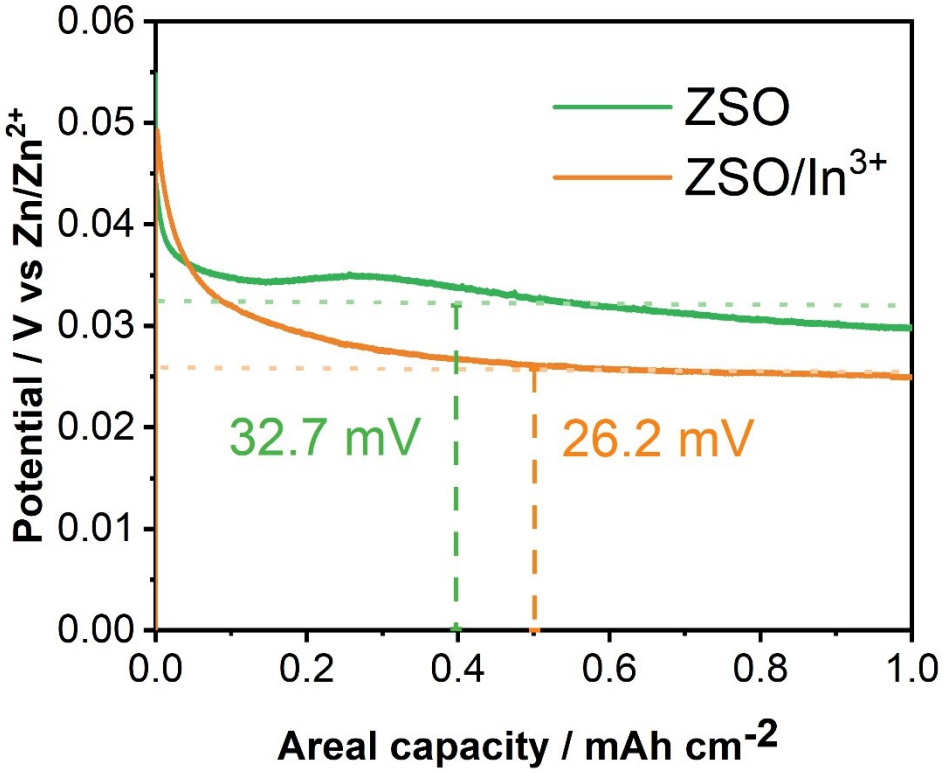

Figure S6 The galvanostatic voltage profiles of a three-electrode system in ZSO and ZSO/In^{3+} at 1 mA cm^{-2} during the Zn stripping process.

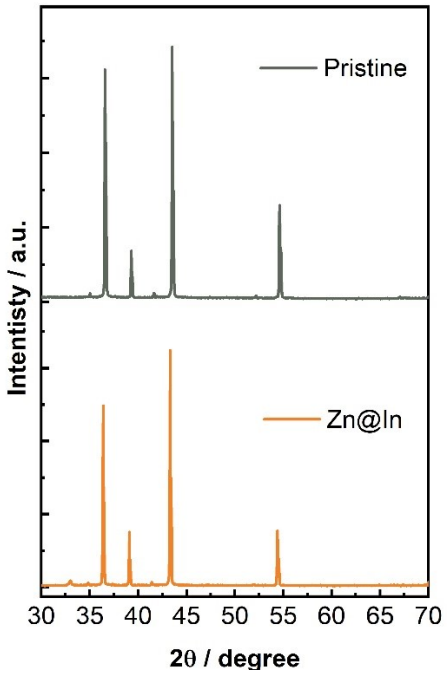

Figure S7. Full-range XRD patterns of pristine Zn and Zn@In electrodes.

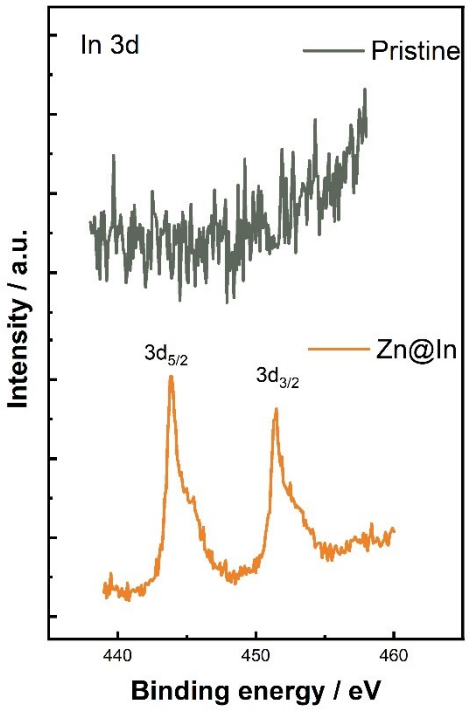

Figure S8. XPS spectra of In 3d for pristine Zn and Zn@In electrodes.

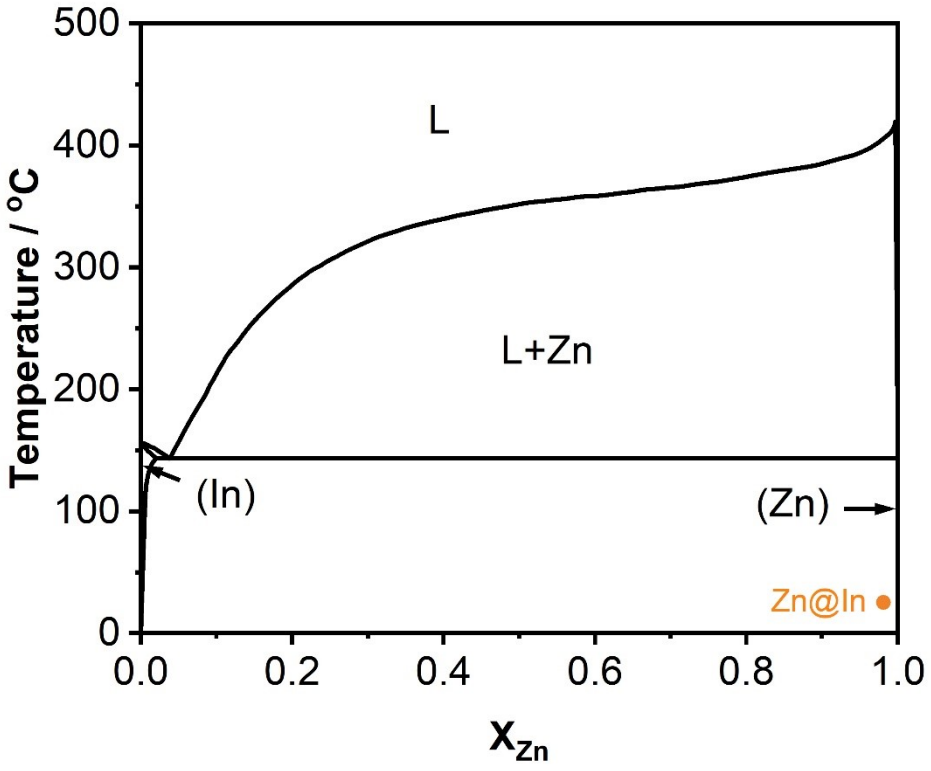

Figure S9. The In-Zn phase diagram.[3, 4]

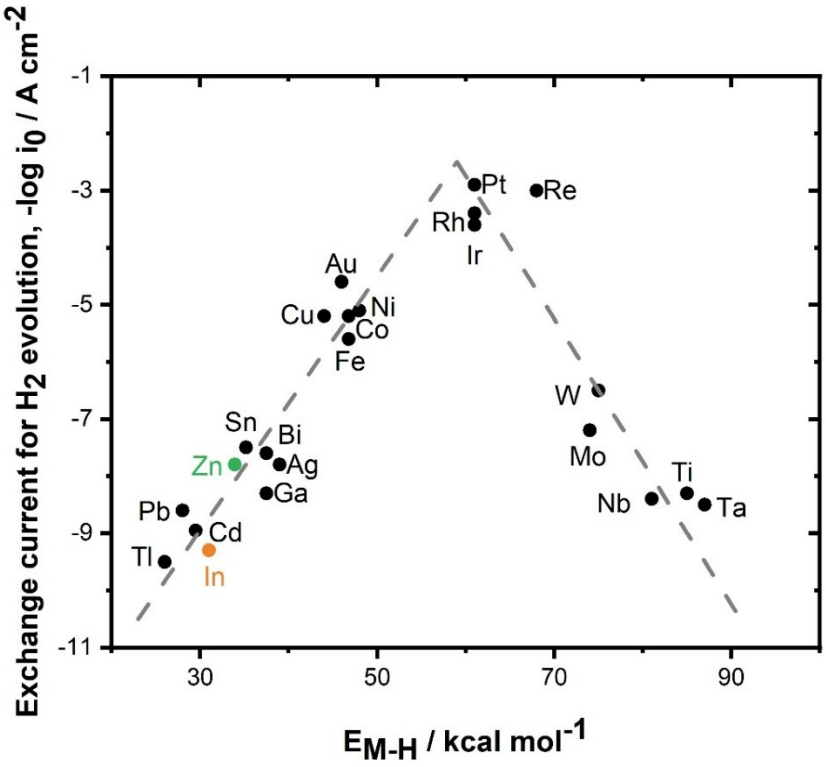

Figure S10. The Trassati's volcano plot for the HER. The exchange current density denotes as i_0, and E_{M_H} represents the intermediate hydrogen-metal bond.[5, 6]

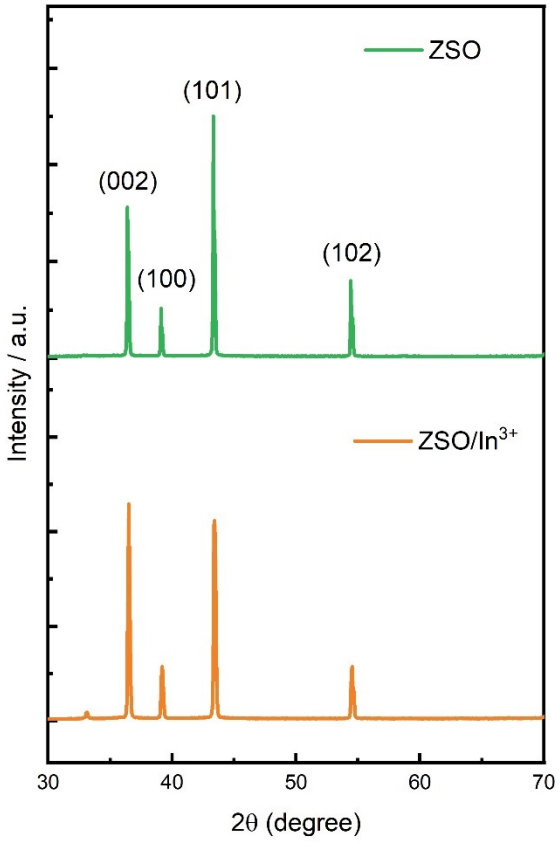

Figure S11. Full-range XRD patterns of Zn electrodes after 40 cycles in ZSO and ZSO/In^{3+} electrolytes.

Relative texture coefficients (RTCs) calculation detail:

To quantitatively evaluate the preferred crystallographic orientation of Zn deposited under various conditions, the relative texture coefficients (RTCs) were calculated from the measured XRD intensities. The RTC values were obtained using:

$$RTC(hkl) = \frac{I_{(hkl)}/I_{0(hkl)}}{\sum(I_{(hkl)}/I_{0(hkl)})} \times 100$$

where I(hkl) is the measured intensity of the (hkl) diffraction plane, and I_0(hkl) represents the corresponding intensity of the standard Zn sample. This ratio directly reflects the relative enhancement or suppression of specific planes after electrochemical cycling.

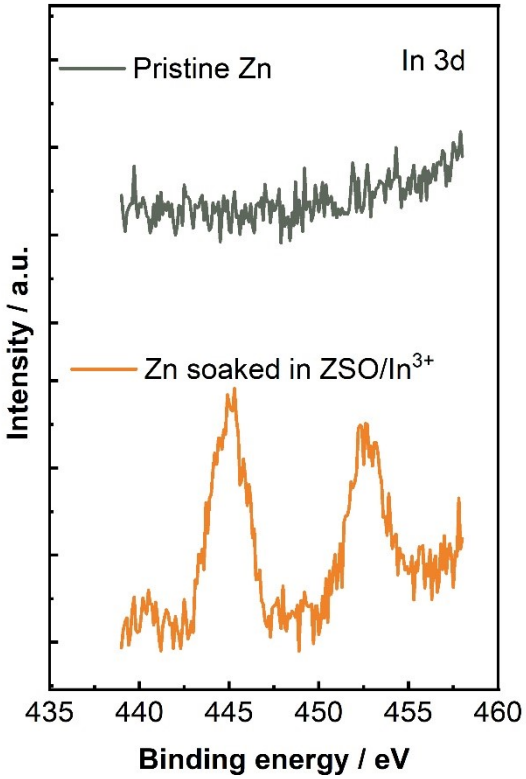

Figure S12. XPS spectra of In 3d for pristine Zn and Zn electrodes soaked in ZSO/In^{3+} electrolytes for 1 h.

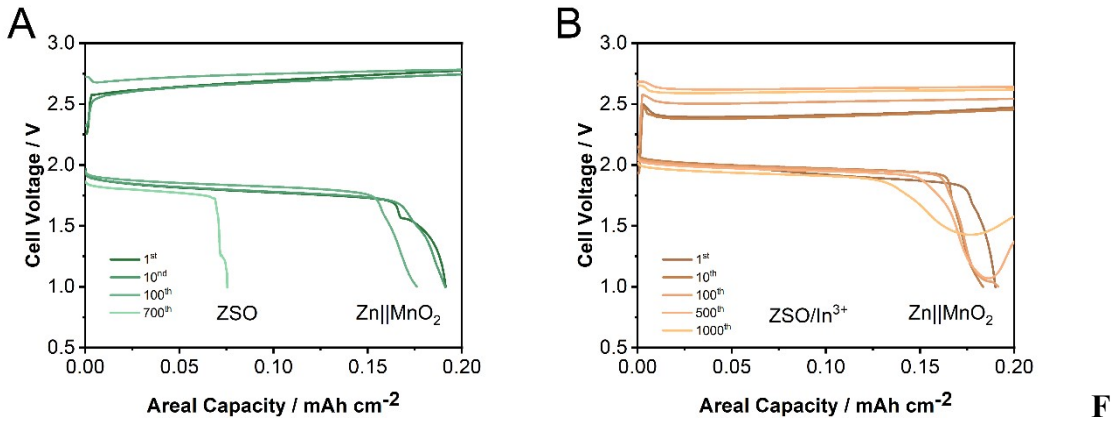

F

igure S13. The galvanostatic charge-discharge voltage profiles of Zn||MnO_2 at 30 mA cm^{-2} charging and 4 mA cm^{-2} discharging with areal capacity 0.2 mAh cm^{-2} over different cycles in (A) ZSO and (B) ZSO/In^{3+} electrolytes.

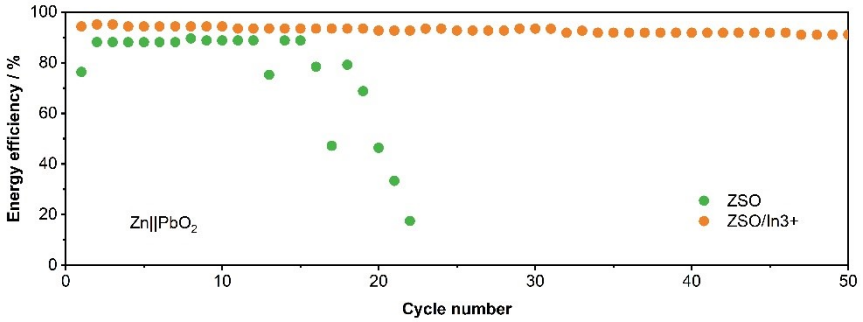

Figure S14. The energy efficiency-cycle profiles of Zn||PbO_2 batteries with ZSO and ZSO/In^{3+} electrolytes at 4 mA cm^{-2} charging and 10 mA cm^{-2} discharging with an areal capacity of 0.5 mAh cm^{-2}.

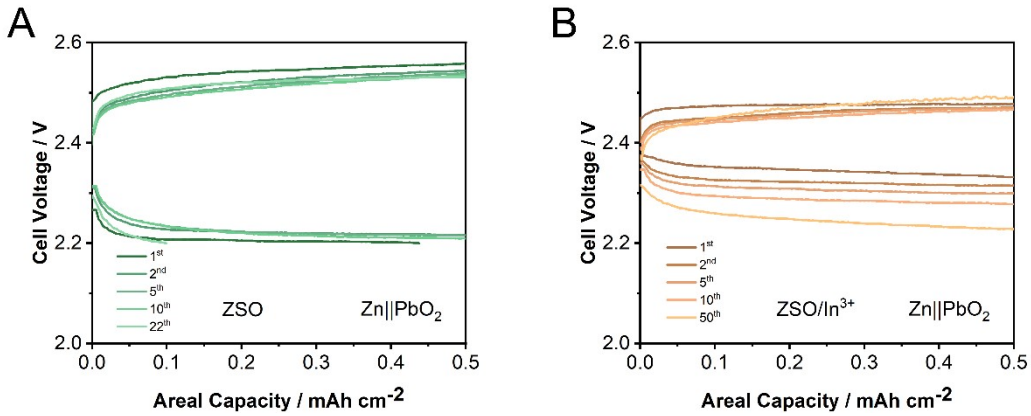

Figure S15. The galvanostatic charge-discharge voltage profiles of Zn||PbO_2 at 4 mA cm^{-2} charging and 10 mA cm^{-2} discharging with areal capacity 0.5 mAh cm^{-2} over different cycles in (A) ZSO and (B) ZSO/In^{3+} electrolytes.

Quantitative analysis of the hydrogen evolution rate:

The hydrogen evolution rate could be assessed based on the electrolyte pH variation during cycling (**Figure 1E**). Since the hydrogen evolution reaction (HER) involves proton reduction ($2H^+ + 2e^- \rightarrow H_2$), the extent of proton consumption provides an indirect measure of hydrogen generation. The estimation of the HER rate is based on the following route:

pH → determination of proton consumption after cycling → moles of H_2 formed → H_2 generation rate

First, pH is converted to the proton concentration:

$$[H^+] = 10^{-pH}$$

Then, let V be the electrolyte volume. The moles of protons consumed during cycling (here evaluated using the pH after 40 cycles) are calculated as:

$$\Delta H^+(mol) = V \cdot [H^+]_{initial} - V \cdot [H^+]_{after\ cycle}$$

This value represents the total amount of protons consumed over 40 cycles and is used to estimate the cumulative hydrogen generation. According to the HER stoichiometry, two protons produce one hydrogen molecule. Thus, the moles of hydrogen formed are:

$$H_2\ gas\ generation\ (mol) = \frac{\Delta H^+(mol)}{2}$$

The hydrogen generation rate is then obtained by normalizing to the cycling time (80 h):

$$H_2\ gas\ generation\ rate\ (mol/hr) = \frac{H_2\ gas\ generation(mol)}{cycled\ time\ (hr)}$$

Table S1. The average hydrogen evolution rates of Zn in ZSO and ZSO/In^{3+}.

	ZSO	ZSO/In^{3+}
Total H_2 gas/mmol	0.208	0.0903
Average HER rate/mmol h^{-1}	0.00259	0.00113

Table S2. Comparisons of the cumulative Zn plating/stripping capacity of symmetric cells employing various Zn electrodes in acidic electrolytes.

Symmetric cell configuration	**Current density (mA cm^{-2})**	**Fixed capacity (mAh cm^{-2})**	**Time (hr)**	**Cumulative capacity (Ah cm^{-2})**	**pH**	**Ref**
Zn |$ZnCl_2$+ Mn(H_2PO_4)$_2$| Zn	1	1	700	0.35	1.9	[7]
PAZn |$ZnSO_4$+ H_3PO_4| PAZn	1	0.5	3600	1.8	2.2	[8]
Zn	5	5	315	0.7875	2.8	[9]

$\|ZnSO_4$+ NHP| Zn						
Zn|$ZnSO_4$+Gly| Zn	4	2	600	1.2	3.5	[10]
Zn |ZnBF-VC| Zn	1	0.5	1000	0.5	3.5	[11]
Zn |$ZnSO_4$+ BT-3| Zn	1	1	2700	1.35	3.8	[12]
Zn |DE| Zn	5	5	260	0.65	5.1	[13]
Zn |Sul/$ZnSO_4$| Zn	10	10	300	1.5	4.2	[14]
Zn |$ZnSO_4$ +$In_2(SO_4)_3$| Zn	**1**	**1**	**2950**	**1.475**	**1.13**	**This work**
Zn |$ZnSO_4$| Zn	**1**	**1**	**60**	**0.03**	**1.13**	**This work**

Table S3. The atomic ratios of Zn and In calculated from XPS data.

	Zn / Atomic %	In / Atomic %
Sample 1	98.3775	1.6225
Sample 2	98.09	1.91
Sample 3	97.92	2.08
Average	98.13	1.87

Quantitative analysis of self-corrosion rate:

The Zn corrosion rate was directly quantified using a gravimetric method based on the mass loss after immersion in different electrolytes (**Figure 4E**). The corrosion rate was calculated from the difference between the initial and remaining masses of the Zn electrode after 48 h immersion and normalized by the immersion time:

$$r_{corr} = \frac{W_0 - W_t}{t}$$

where r_{corr} is the corrosion rate (mg h^{-1}), W_0 is the initial mass of the Zn electrode (mg), W_t is the remaining mass after immersion (mg), and t is the immersion duration (h), which was fixed to be 48 h.

Table S4. The average corrosion rates of Zn in ZSO and ZSO/In^{3+}.

	W_0 / mg	**W_t / mg**	**Mass loss / mg**	**Corrosion rate / mg h^{-1}**
Zn in ZSO / mg	80.8	46.7	34.1	0.710
Zn in ZSO/In^{3+} / mg	79.7	72.1	7.6	0.158

Table S5. Comparisons of electrochemical performance of ZIBs assembled in coin-cell formats applying various electrolyte/additive strategies.

Cathode	**Electrolyte**	**Cycle number**	**Plateau Cell Voltage(V)**	**Ref**
$LiFePO_4$	2 M ZSO4 +2 g/L $CeCl_3$	400	1.1	[15]
$NH_4V_2O_5$	2 M $ZnSO_4$ + 100 mM MAPTAC	1000	0.65	[16]
V_2O_5	1 m $Zn(CF_3SO_3)_2$+50 mg mL^{-1} dextran	600	0.8	[17]
V_2O_5	2 M $ZnSO_4$ + 50 mM polyhydroxy (Sucral)	500	0.75	[18]
MnO_2	2 m $ZnSO_4$ + 0.2 wt% Fumed silica (FS)	1000	1.3	[19]
MnO_2	2 M $ZnSO_4$ + 2 mM penta-potassium triphosphate	300	1.3	[20]
MnO_2	2 M $ZnSO_4$ + 80 mM sodium methylenedinaphthalene disulphonate (SMD)	200	0.75	[21]
Graphite	**1 M $ZnSO_4$+1M $MnSO_4$+5mM $In_2(SO_4)_3$**	**1100**	**1.9495**	**This work**

References:

1. C. C. L. McCrory, S. Jung, J. C. Peters and T. F. Jaramillo, *Journal of the American Chemical Society*, 2013, **135**, 16977–16987.
2. S. Trasatti and O. A. Petrii, *Pure and Applied Chemistry*, 1991, **63**, 711–734.
3. J. Pstruś, Z. Moser and W. Gąsior, *Applied Surface Science*, 2011, **257**, 3867–3871.
4. J. Dutkiewicz and W. Zakulski, *Bulletin of Alloy Phase Diagrams*, 1984, **5**, 284–289.
5. P. Quaino, F. Juarez, E. Santos and W. Schmickler, *Beilstein Journal of Nanotechnology*, 2014, **5**, 846–854.
6. S. Trasatti, *Journal of Electroanalytical Chemistry and Interfacial Electrochemistry*, 1972, **39**, 163–184.
7. Y. Liu, Z. Qin, X. Yang, J. Liu, X.-X. Liu and X. Sun, *ACS Energy Letters*, 2022, **7**, 1814–1819.
8. H. Yang, L. Li, D. Chen, J. Wang, Y. Tan, Z. Jiang, Y. Zhang, C. Miao, W. Zhang and W. Han, *Angewandte Chemie*, 2025, **137**, e202419394.
9. W. Zhang, Y. Dai, R. Chen, Z. Xu, J. Li, W. Zong, H. Li, Z. Li, Z. Zhang and J. Zhu, *Angew. Chem. Int. Ed.*, 2023, **62**, e202212695.
10. Q. Gou, H. Luo, Q. Zhang, J. Deng, R. Zhao, O. Odunmbaku, L. Wang, L. Li, Y. Zheng and J. Li, *Small*, 2023, **19**, 2207502.
11. S. Wang, Y. Ying, S. Chen, H. Wang, K. K. K. Cheung, C. Peng, H. Huang, L. Ma and J. A. Zapien, *Energy Storage Materials*, 2023, **63**, 102971.
12. Y. M. Li, W. H. Li, X. Y. Zhang, Y. Z. Tang, Z. M. Liu, J. P. Zhang and X. L. Wu, *Advanced Functional Materials*, 2025, **35**, 2420446.
13. R. Chen, W. Zhang, Q. Huang, C. Guan, W. Zong, Y. Dai, Z. Du, Z. Zhang, J. Li and F. Guo, *Nano-Micro Letters*, 2023, **15**, 81.
14. C. Huang, X. Zhao, Y. Hao, Y. Yang, Y. Qian, G. Chang, Y. Zhang, Q. Tang, A. Hu and X. Chen, *Energy & Environmental Science*, 2023, **16**, 1721–1731.
15. Z. Hu, F. Zhang, Y. Zhao, H. Wang, Y. Huang, F. Wu, R. Chen and L. Li, *Advanced Materials*, 2022, **34**, 2203104.
16. Y. Wang, Y. Zhang, H. Ye, M. Wei, Y. Gu, K. Hu, S. Qu, R. Wu, X. Li, J. Zhang, C. Liu, D. Jia and H. Lin, *Small*, 2025, **21**, e09465.
17. J. Li, Z. Guo, J. Wu, Z. Zheng, Z. Yu, F. She, L. Lai, H. Li, Y. Chen and L. Wei, *Advanced Energy Materials*, 2023, **13**, 2301743.
18. Q. Zhao, W. Liu, X. Ni, H. Yu, C. Zhang, B. Wang, L. Jiang, H. He, Y. Chen and L. Chen, *Advanced Functional Materials*, 2024, **34**, 2404219.
19. R. Wang, J. Zhu, M. Yang and Z. Niu, *Angewandte Chemie International Edition*, 2025, **64**, e202501327.
20. Y. Yu, P. Zhang, W. Wang and J. Liu, *Small Methods*, 2023, **7**, 2300546.
21. S. Zheng, Y. Wang, B. Luo, L. Sun, G. Duan, J. Huang and Z. Ye, *Chemical*

Engineering Journal, 2023, **473**, 145313.